energies

MDPI

Article

Strategy for Suppressing Commutation Failures in High-Voltage Direct Current Inverter Station Based on Transient Overvoltage

Dandan Zhao [1], Shaoyin He [2,*], Hua Huang [1], Zheng Han [1], Lv Cui [1] and Yuxin Li [2]

[1] Equipment Technology Center, State Grid Shanghai Electric Power Research Institute, Shanghai 200437, China; zhaodd_xjtu@163.com (D.Z.); huahuang@sina.com (H.H.); han5104@163.com (Z.H.); cuil@sh.sgcc.com.cn (L.C.)

[2] State Key Laboratory of Electrical Insulation and Power Equipment, School of Electrical Engineering, Xi'an Jiaotong University, Xi'an 710049, China; yuxinli@stu.xjtu.edu.cn

* Correspondence: shaoyin.he@xjtu.edu.cn

Abstract: Commutation failures in high-voltage direct current (HVDC) transmission systems often occur within inverter stations, posing challenges to the safe and consistent operation of HVDC transmission projects. This paper examines data gathered from a wide-spectrum transient electromagnetic voltage monitoring apparatus. The findings uncover a notable correlation between transient AC bus voltage disturbances, stemming from faults, and the occurrence of commutation failures in HVDC transmission systems. Leveraging this correlation, we propose a commutation failure mitigation strategy for HVDC systems centered around AC bus voltage disturbances within inverter stations. Through fault validation simulations conducted across three HVDC transmission systems, our strategy demonstrates effective suppression of commutation failure incidents within HVDC transmission projects.

Keywords: HVDC; commutation failure; transient voltage disturbance; broadband voltage measurement; suppression strategy

Citation: Zhao, D.; He, S.; Huang, H.; Han, Z.; Cui, L.; Li, Y. Strategy for Suppressing Commutation Failures in High-Voltage Direct Current Inverter Station Based on Transient Overvoltage. *Energies* **2024**, *17*, 1094. https://doi.org/10.3390/en17051094

Received: 19 December 2023
Revised: 13 February 2024
Accepted: 16 February 2024
Published: 25 February 2024

1. Introduction

High-voltage direct current (HVDC) transmission offers significant advantages, including extended transmission distances, enhanced transmission capacity, and reduced line losses, making it an effective solution for addressing energy distribution imbalances [1–3]. Notably, in the Yangtze River Delta, an ultra-high-voltage multi-drop AC/DC hybrid power grid has been established. The proliferation of DC lines results in the formation of a multi-infeed HVDC system, enhancing grid operational flexibility but, concurrently, imposing heightened stability requirements [4–7]. Commutation failure (CF) stands as a prevalent fault encountered on the inverter side of HVDC transmission systems. It can trigger voltage fluctuations and power drops and even lead to DC block in cases of continuous multiple failures [8–10]. This interconnected AC/DC power grid is particularly sensitive to the status of the DC system, directly impacting the overall safety and stability of the grid. Key contributors to CF encompass reductions in the AC bus voltage, distortions arising from grounding faults within the AC system at the inverter side, and the switching of high-capacity equipment [11,12].

Several studies have delved into the mechanism of CF and suggested suppression measures [13,14]. For instance, a novel approach employing a thyristor-based controllable capacitor was introduced in reference [15], targeting CF elimination, especially in higher-power/current LCC HVDC systems. The efficacy of CF mitigation often faces constraints due to the delay in extinction angle (EA) measurement or inaccuracies in existing prediction methods for EA or firing angle (FA). To address this, ref. [16] proposed a CF mitigation technique founded on the conceptualization of the imaginary commutation process. The author of [17] introduced a CF prevention control module capable of swiftly recognizing

faults. This method enhances the lead trigger angle by detecting zero-sequence voltage and AC voltage amplitude variations. This method effectively suppresses CF occurrences. Similarly, in [18], a control strategy was proposed to curtail continuous CF by reducing the lead trigger angle's fluctuation range. By establishing compensation components through hysteresis comparisons based on the disparity between the actual and commanded trigger angles, control over the lead trigger angle's fluctuation range is achieved. Some scholars introduced a CF suppression method centered on diminishing control angle errors using phase-locked loop transient error measurements. Moreover, in [19], a conventional predictive control approach involving constant extinguish angle control was enhanced using a DC current prediction module. This method optimizes the controller by establishing the minimum trigger angle of each valve as the definitive output command, consequently decreasing the likelihood of CF occurrences [20].

The research achievement described above have enabled a certain degree of CF suppression. Although the commutation failure suppression method mentioned in the above literature has achieved a certain effect of inhibiting commutation failure, it is difficult to meet the actual engineering requirements due to the feedback signal delay. Therefore, to optimize a CF suppression strategy, it is crucial to understand the relationship between the transient electromagnetic characteristics of AC bus fault voltage and CF generation mechanisms. We assess the correlation between CF and AC bus voltage attributes using data captured by a broadband transient electromagnetic voltage online monitoring device. Additionally, we introduce a mitigation strategy aimed at averting commutation failures in HVDC systems, focusing on disturbances within inverter station AC bus voltages.

2. Correlation Analysis of Electromagnetic Disturbance and Commutation Failure

2.1. Commutation Failure Mechanism

The converter valve of a traditional HVDC transmission system utilizes a semi-controlled thyristor. Following conduction, the thyristor requires a specific duration to complete carrier recombination. This duration, termed the recovery time of the thyristor valve, is denoted in electrical terms as γ_{min}. Commutation between two bridge arms may lead to commutation failure (CF) if the valve does not regain its blocking ability within the timeframe before the reverse voltage acts. Essentially, CF occurs if the inverter turn-off angle γ is shorter than the recovery time of the thyristor valve γ_{min} in this scenario. The turn-off angle can be calculated using (1):

$$\gamma = \arccos\left(\frac{2I_d X_r}{U_L} + \cos\beta\right) \quad (1)$$

where I_d is the DC current flowing through the converter valve; U_L is the commutation voltage; X_r is the commutation reactance; and β is the leading trigger angle of the converter valve. According to (1), reducing the AC bus voltage and trigger lead angle or increasing the DC current and commutation reactance will decrease the turn-off angle and risk of CF.

2.2. Wideband Measurement System for Transient Electromagnetic Voltage

The capacitive voltage divider (CVD) used in these tests has been designed for measuring high-frequency fault transients across various apparatuses like power transformers, instrument transformers, switchgear, breakers, and HV cables. It adheres to all the requirements outlined in IEC 60060-2, particularly in terms of measuring accuracy and step response. This ensures high reliability and robust voltage sensing, minimizing interference. The inductive-free broadband sensing unit connects the medium-voltage capacitor and the ground to create a high-voltage capacitive voltage divider [21]. Figure 1 illustrates the structure of this equipment. The monitoring device's 3 dB cutoff frequency is higher than 200 kHz, which can respond to lightning voltage impulse responses and transient overvoltage with a microsecond-order rising time.

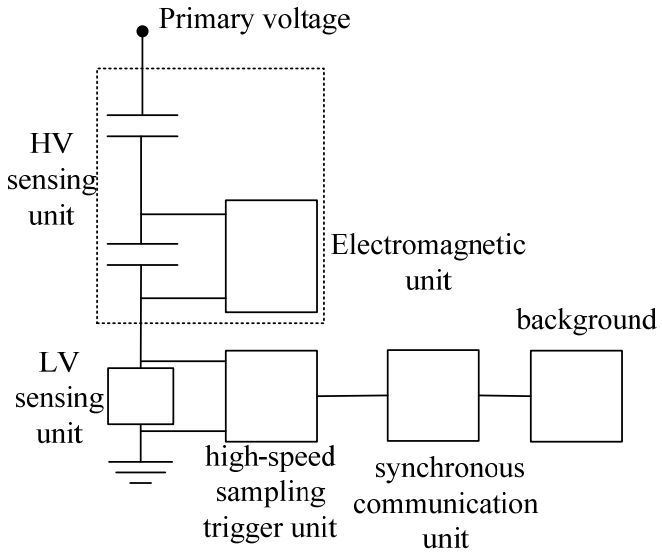

Figure 1. The schematic circuit diagram of CVD.

2.3. Measurement of AC Transient Voltage Disturbance

To the best of our knowledge, there are no comprehensive studies of the AC voltage disturbance characteristics of converter stations. The measured disturbances only include transient voltages that have caused CF. This makes it difficult to determine the frequency and nature of AC voltage disturbances that cause CF. Herein, we propose a trigger mode for the transient voltage disturbance of periodic signals. Specifically, by recording the transient voltage disturbances whose amplitude and duration meet the designated conditions, it is possible to detect small signal voltage disturbances near the zero-crossing point. The trigger source y is defined as

$$y = \Sigma \left| u_k - u_{k-T} \right| \quad (2)$$

where u_k and u_{k-T} are the disturbance of transient voltage in a period T, k presents the different phase voltage identification of AB, BC, or CA. When y is greater than the trigger threshold, the system is triggered to record the wave data.

We investigate the characteristic of electromagnetic disturbance which pass through one side of the transformer to the other side. A short-circuit fault on the 220 kV power system causes a voltage disturbance on the 500 kV power system due to the interaction of the voltages on both sides of the transformer. The sensor is not only sensitive to voltage disturbances caused by faults in the 500 kV power system, but also has some applicability to crossing voltage disturbances caused by faults in the 220 kV power system or the 1000 kV power system on the 500 kV power system. The top picture in Figure 2 displays the three-phase voltage waveforms as measured by the sensor, while the bottom graph illustrates the voltage disturbance waveform in the time domain, representing the occurrence of the disturbance phase. In this example, the system voltage disturbance time is $t_0 = 9878.06$ μs, the trigger signal jump time is $t_1 = 9992.75$ μs, and the actual trigger time is $t_2 = 10,000$ μs. Various voltage disturbances were measured by the monitoring device, such as a single-phase fault, a two-phase grounding fault, a closing no-load line, a switching filter, etc. The typical voltage waveform of a 500 kV system with a single-phase grounding fault is shown in Figure 3.

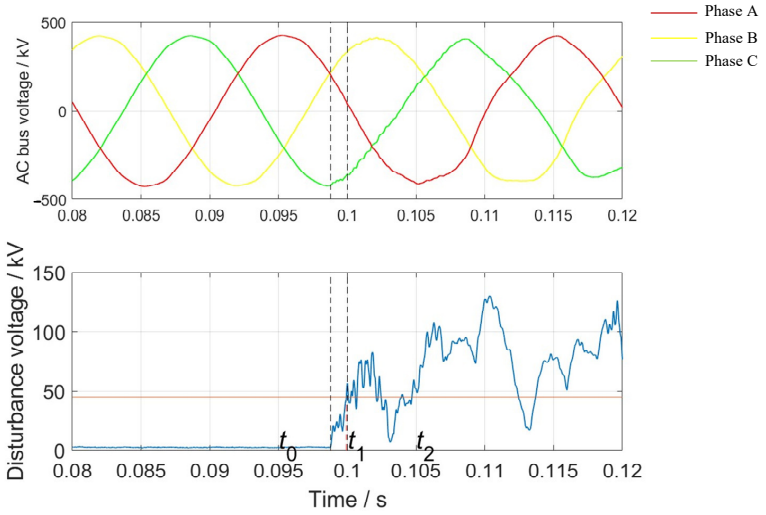

Figure 2. Measured voltage transient disturbance.

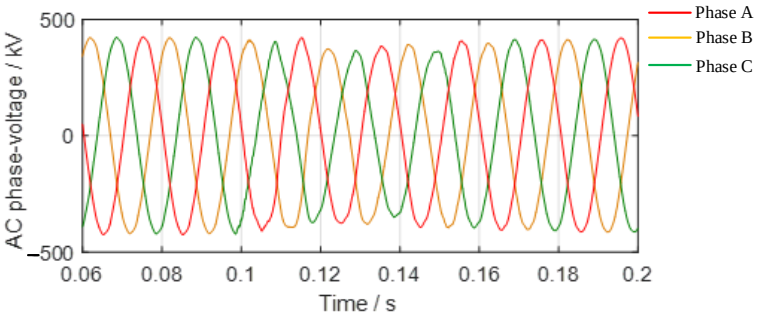

Figure 3. Typical 500 kV system voltage with single-phase grounding fault measured by the monitoring device.

2.4. Time Integral of Disturbance Voltage

The commutation area is a parameter representing the commutation voltage. If the voltage time area is too small during commutation, this will result in CF. However, during AC voltage wave recording, the state of the DC operation cannot be considered. Therefore, we propose to use the time integral of the disturbance voltage to characterize the severity of AC voltage disturbance [22]. The time integral of the disturbance voltage is equal to the change in AC voltage relative to the previous cycle. The relationship between the time integral of the disturbance voltage and the commutation area is significant in terms of analyzing the disturbance characteristics of the AC power grid in an AC/DC hybrid power grid. The time integral of the disturbance voltage is defined in (3):

$$S = \int_{t_0}^{t_0+T} \left| u_k - u_{k-n_T} \right| dt \tag{3}$$

where t_0 is the disturbance occurrence time; T is the power frequency cycle; and n_T is the sampling point corresponding to a period in the power frequency.

2.5. Correlation Analysis of AC Voltage Disturbance and DC Commutation Failure

The device recorded 280 transient voltage disturbance events with identifiable sources, predominantly involving filter switching, faults, main transformer switching, no-load line switching, main transformer low-voltage capacitor switching, and disruptions from the DC system. Among these events, a total of 89 commutation failures occurred in the converter station.

Figure 4 displays the box diagram of the time integral of voltage disturbance concerning the occurrence of CFs. The maximum value for a voltage disturbance time integral without CFs is 0.27, whereas the minimum value associated with CFs is 0.45. This indicates that, in the exemplary Fengjing converter station, there are specific thresholds for the time integral of AC voltage disturbances that could potentially cause CFs, distinguishing them from transient voltage disturbances which cannot. Notably, there are 15 outliers, accounting for approximately 6.4% of the cases without CFs, necessitating further investigation. However, these outliers have a minimal impact on the overall results. The outcome distinguishes the effect of AC voltage disturbance on the occurrence of a CF in the DC system, denoted by the binary state variable [0 1], where 0 represents no CF occurrence and 1 indicates a CF occurrence. The Spearman correlation coefficient between transient voltage disturbance and CF registers at 0.65, suggesting a strong correlation between the two factors. The red lines represent outliers.

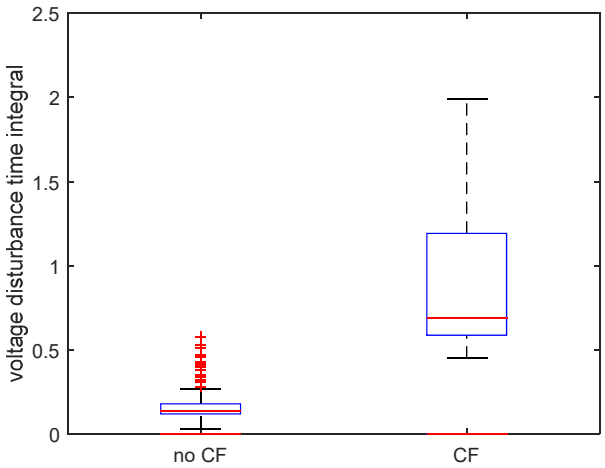

Figure 4. Box diagram of voltage disturbance time integral.

3. Predictive Logic for Commutation Failure

The DC transmission control system serves three purposes. First, it can keep DC power, voltage, current, and control angle within steady-state values. Second, it can limit transient overvoltage and overcurrent. Finally, after failure of the AC and DC systems, it responds quickly and resumes power delivery smoothly. The control system of an HVDC transmission system contains four levels, which are the system control level, the pole control level, the converter control level, and the valve control level. The higher the control level, the slower the response speed. Among them, converter control is the foundation. It completes the control of a DC current through the control of the converter trigger pulse; then, it controls the transmission power. During normal operation, the DC control system should control the DC power, DC voltage, and DC current within the steady-state range.

Given the stringent demands for response time in a DC control system, we propose a CF prediction method centered on AC bus voltage disturbance (shown in Figure 5). The fundamental objective of this approach is to detect any fluctuations in AC bus voltage. Once the disturbance surpasses a predefined threshold, the trigger angle is modulated, with the degree of adjustment contingent upon the magnitude of the AC voltage shift [23].

The function of commutation failure prevention (CFPREV) control is to instantaneously increase the commutation margin in the event of an AC system fault. The zero-sequence voltage component is obtained by summing three-phase AC phase-change voltages. The instantaneous AC voltage magnitude is obtained by α/β transformation. When the discriminative condition of a single-phase or three-phase AC fault is satisfied, an alpha variation in CFPREV control is output. CFPREV control can effectively avoid commutation failure caused by mild AC faults.

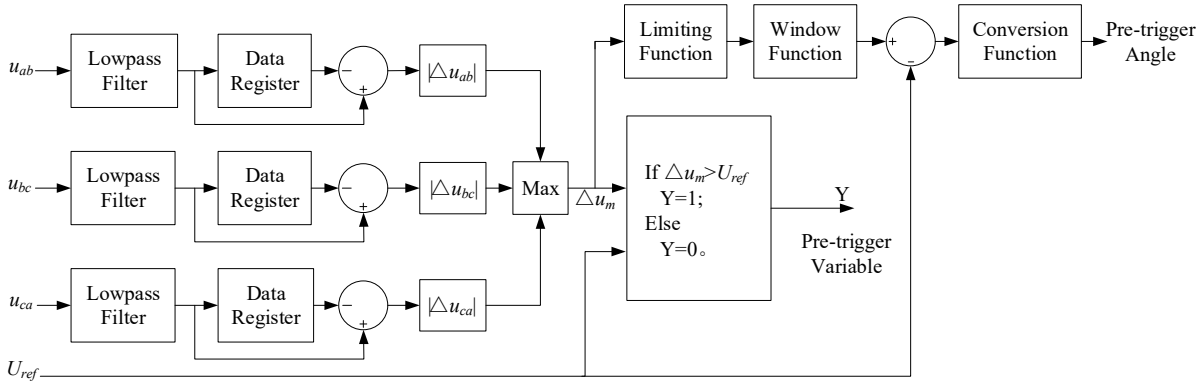

Figure 5. Block diagram of the CF suppression strategy based on AC bus voltage disturbance.

Based on the operational experience and long-term data accumulation of the Chinese HVDC transmission system from Tuanlin to Fengjing, the paper proposes a predictive algorithm to prevent commutation failures in LCC-HVDC systems for optimizing existing control and protection strategies. The algorithm is also validated in the Fulong-to-Fengxian and Yidu-to-Huaxin HVDC projects. The basic logic of the algorithm involves the online monitoring of AC bus voltage disturbances. When the voltage disturbance exceeds a predefined threshold, the algorithm triggers control variables in advance and adjusts the triggering angle of the converter valves accordingly. The specific algorithm steps are described as follows:

1. Online monitoring and recording of inter-phase voltages are conducted, with high-frequency noise interference filtered out by a filter. This algorithm only considers operational and fault transient voltage disturbances that can cause commutation failures, while transient disturbances of higher frequencies such as lightning and very fast transient overvoltage (VFTO) are not within the scope of this optimization strategy. Therefore, a cutoff frequency of 10 kHz or higher can be set as the high-frequency cutoff frequency (or adjusted according to the specific conditions of the converter station).
2. Using data registers to store the waveform data from the previous cycle, perform a differential operation between the current waveform data and the previous cycle's data to calculate the absolute difference of the inter-phase voltages in the current cycle and the previous cycle, denoted as $|\Delta U_{AB}|$, $|\Delta U_{BC}|$, and $|\Delta U_{CA}|$. Then, determine the maximum value among these three voltage disturbances, denoted as ΔU_m.
3. Based on the specific requirements of the DC transmission project, set the threshold voltage disturbance value ΔU_{m_ref}. When $\Delta U_m > \Delta U_{m\_ref}$, set the trigger control variable Y within the control and protection system to 1. Otherwise, set Y to 0 and output Y.
4. In addition to setting the advance trigger variable Y, another function of the optimization logic is to calculate the advance trigger angle. The disturbance amplitude ΔU_m is converted into an angle output as the trigger angle through an angle conversion function. The role of the amplitude limiting function is to constrain ΔU_m within a reasonable range, with specific values adjusted based on historical data and protection system requirements. The window function sets the duration of recorded data to a finite time window, typically one cycle based on our operational experience, not exceeding two cycles, i.e., 20–40 ms. The window function ensures that our strategy only targets the initial voltage drop stage during fault inception, while ignoring disturbances caused by voltage rise after the protection system's operation.
5. The flow diagram of the CF suppression strategy is shown in Figure 5.

4. Simulation Verification Based on Typical Control and Protection Systems

Fault-scanning simulations were conducted using three distinct control systems: the standard CIGRE HVDC system, the XJ-SIMENS control system (Linfeng HVDC projects), and the NARI-ABB control system (Fufeng HVDC projects). These simulations utilized fault impedance, representing grounding impedance, and considered the distance from the fault point to the converter station. The fault inductance (L_g) range varied across different projects. The simulations accounted for an average fault time interval of 10 points within half a cycle, set at an interval time of 0.001 s, corresponding to an angle of 18°.

4.1. Validation of CIGRE Simulation Models

A standard CIGRE HVDC test system is depicted in Figure 6. The AC system in the inverter station has a short-circuit ratio of 2.5. In the event of a single-phase grounding fault in the AC system, the converter station's bus voltage undergoes significant distortion, distinguishing it from the measured fault voltage waveform. Typically, China's HVDC transmission systems feature a robust AC power grid on the inverter side, with a substantial short-circuit ratio. To enhance the generalizability of our research findings, we made a slight adjustment to the AC system model on the inverter side of the standard CIGRE HVDC test system: specifically, the removal of the 36.5 mH series inductance in front of the inverter-side power supply. The Short Circuit Ratio (SCR) of the inverter is the ratio of the short circuit current of the output voltage of the inverter to the rated output current. Following this modification, the SCR of the AC system on the inverter side became 5. Under the same ground fault scenario, the key characteristics of the inverter station's AC bus voltage, illustrated in Figure 7, closely resemble the features of the measured fault voltage waveform (Figure 3).

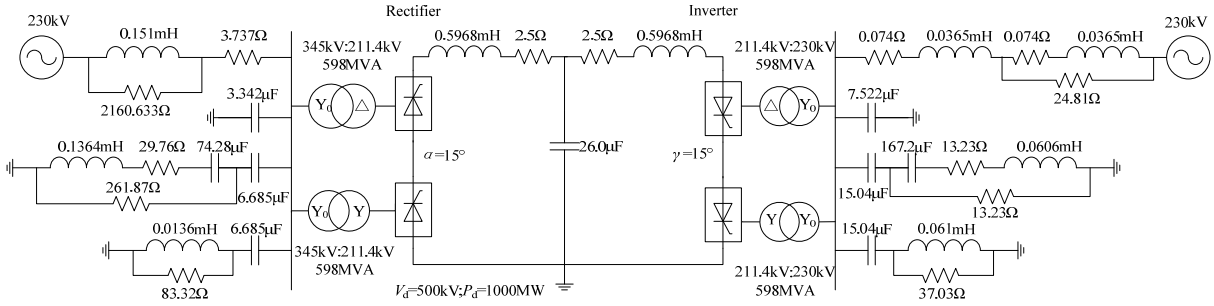

Figure 6. Standard CIGRE HVDC test system.

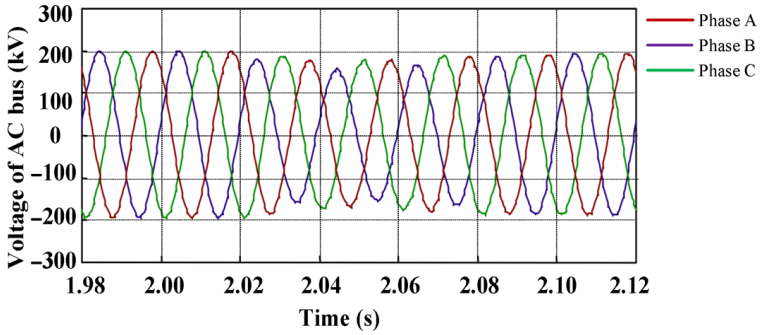

Figure 7. Voltage waveform of a single-phase grounding fault in the inverter station AC bus in the modified standard CIGRE HVDC test system.

Within the standard CIGRE HVDC test system, the prediction step has an upper amplitude threshold of 0.4 and a lower limit of 0. The DC current remains at its rated level, and the fault inductance range, L_g, spans from 0 to 0.60 H.

The simulation outcomes (Figure 8) demonstrate that, prior to initiating the prediction step, CFs occurred in 76 instances. After implementing the prediction step, this count reduced to 33, marking a substantial 56.6% decrease and confirming its efficacy in CF prevention.

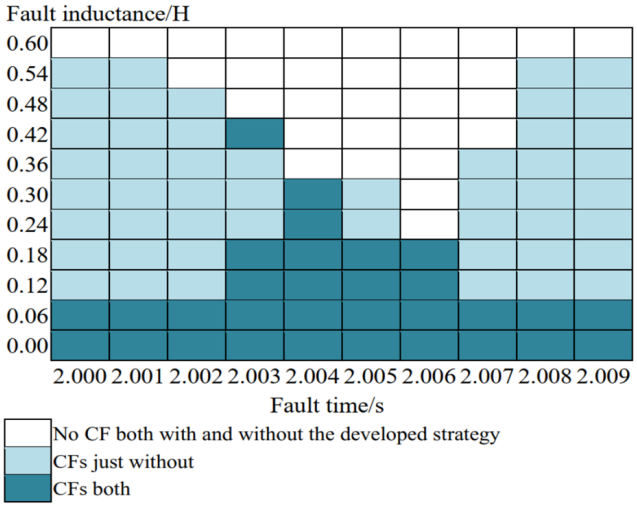

Figure 8. Results of the proposed strategy with the standard CIGRE HVDC test system.

Furthermore, in scenarios where a metallic short-circuit fault arises near the AC bus within the standard CIGRE HVDC test system, multiple CFs occurred (up to four occurrences). However, upon integrating the prediction step, there was notable improvement, with a reduction in the frequency of repeated CFs and a decrease in the instances of continuous CFs (now up to three occurrences).

When the fault reactance was 0.24 H and the fault time was set to 2.002 s, the start time of the prediction step was 2.00375 s, and the maximum output was 0.32 rad. Figure 9 illustrates a comparison of the arc extinction angle behavior of the CIGRE HVDC standard test system before and after the introduction of this prediction step. Before implementing this prediction step, the arc extinction angle started to decline at 2.00475 s, dropped to zero at 2.009 s (where the DC system experienced commutation failure), and began to recover after 395 ms. After introducing this prediction step, the arc extinction angle also started to decline at 2.00475 s but reached a minimum value of 11.26° at 2.006 s and began to recover after 165 ms. Figure 10 shows a comparison of the trigger angle behavior of the CIGRE HVDC standard test system before and after the introduction of this prediction step. Before the action of the system's proportional-integral controller, this prediction step had already issued an advance trigger command, successfully preventing the occurrence of this commutation failure event.

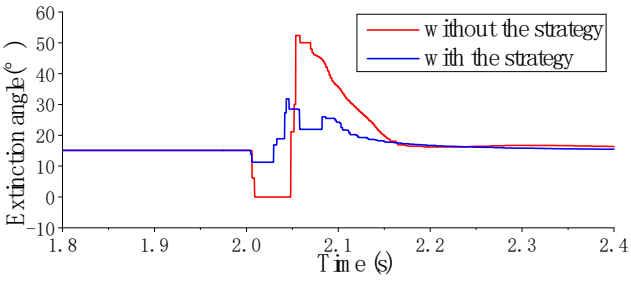

Figure 9. Arc extinction angle curves of the standard CIGRE HVDC test system with and without the developed strategy (Lg = 0.24 H).

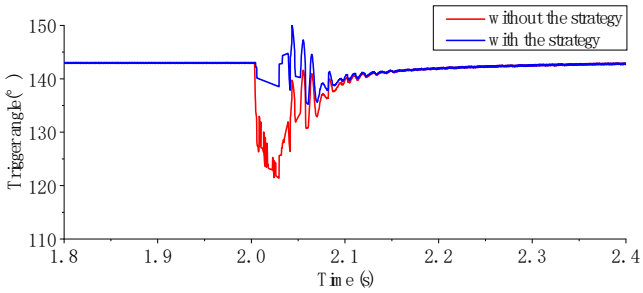

Figure 10. Trigger angles of the standard CIGRE HVDC test.

4.2. Simulation Verification for the Linfeng HVDC Project

In the Linfeng HVDC transmission project, commutation failure incidents are more frequent, and faults in the 220 kV, 500 kV, and 1000 kV systems can potentially lead to commutation failures in the DC system. This study considered these three voltage levels separately during simulations. In the Linfeng HVDC transmission project, the start threshold of the prediction step is $\Delta U_{m\_ref} = 0.13$, with an upper limit of 0.25 and a lower limit of 0 for the amplitude. The DC current is at the rated current level. If the fault originates in the 220 kV system, the fault inductance ranges from 0.3 to 50.3 mH. For faults in the 500 kV system, the fault inductance ranges from 0.3 to 100.3 mH. For faults in the 1000 kV system, the fault inductance ranges from 0.3 to 800.3 mH. The overall simulation results are depicted in Figure 11. Figure 12 illustrates the simulation results specifically when the fault source is in Phase A of the 500 kV system.

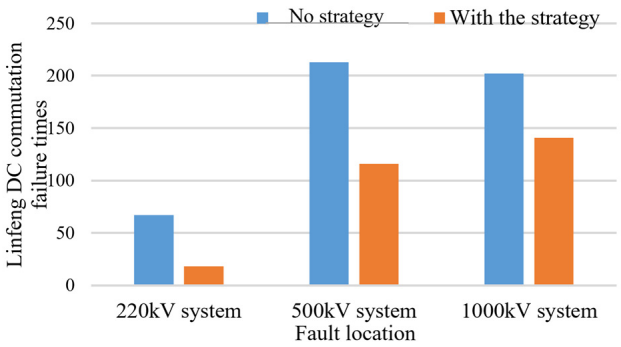

Figure 11. Overall results of the developed strategy in the Linfeng HVDC system.

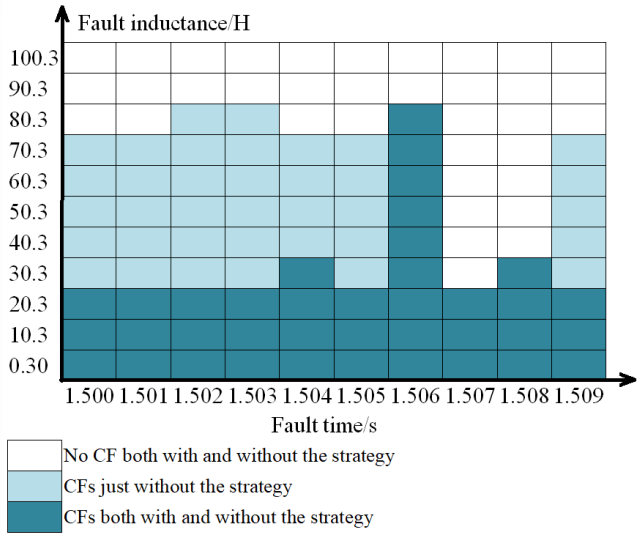

Figure 12. Results of the developed strategy in the Linfeng HVDC system (faults in a 500 kV system).

According to the simulation results, in cases where faults originate in the 220 kV system, overall, the prediction step can reduce 73% of commutation failure incidents, exhibiting a good preventive effect. Particularly for faults occurring before the peak, the preventive effect is exceptional, reducing 90% of commutation failure incidents. For faults originating in the 500 kV system, the prediction step can generally reduce 45% of commutation failure incidents, displaying a good preventive effect. However, its effectiveness is primarily concentrated on faults occurring before the peak; for faults occurring after the peak, the preventive effect is less prominent. The situation with faults originating in the 1000 kV system is similar to that in the 500 kV system.

4.3. Simulation Verification for the Fufeng HVDC Project

In the Fufeng HVDC Transmission Engineering project, the starting threshold of the prediction step is $\Delta U_{\mathrm{m\_ref}} = 0.1$. The upper limit for the amplitude is 0.6, and the lower limit is 0. The fault source is set in the 500 kV system, and the range for fault inductance is 0 to 130.0 mH. The simulation results are shown in Figure 13.

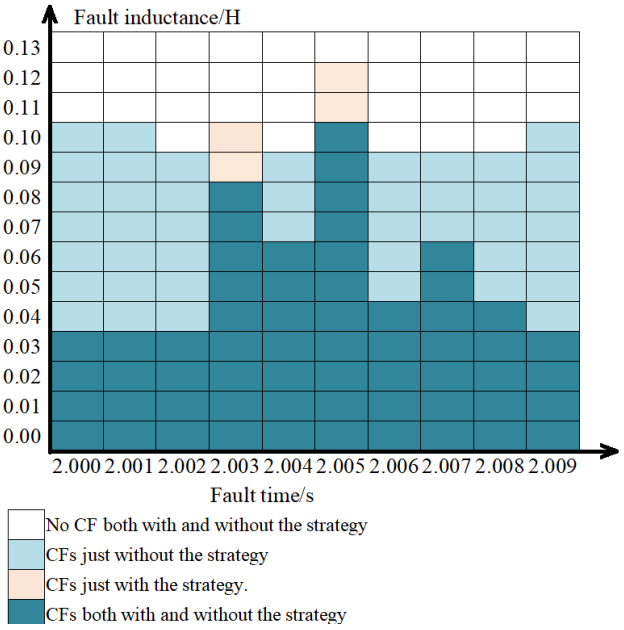

Figure 13. Results of the developed strategy in the Fufeng HVDC system.

In the current Fufeng HVDC station, there is already a prediction step for commutation failure. Therefore, this paper considered multiple combinations. According to the simulation results, if the commutation failure prediction step is not activated, there are a total of 102 scenarios resulting in commutation failures. With only the original prediction step activated, there are 77 scenarios leading to commutation failures, including 6 additional scenarios. When both the original and the proposed prediction steps are activated, the scenarios causing commutation failures decrease to 58, with an additional 6 scenarios. Solely activating the proposed prediction step reduces the scenarios causing commutation failures to 64, with 4 additional scenarios. The simulation results for this scenario are shown in Figure 13. Through a comparative analysis, it is observed that solely activating the proposed prediction step reduces the occurrences of commutation failures in the Fufeng HVDC system by 37.3%. Hence, the commutation failure prediction step proposed in this paper exhibits a favorable effectiveness in the Fufeng HVDC project.

5. Influence Analysis for Commutation Failure Suppression Effectiveness

Based on the analysis above, the commutation failure prediction strategy proposed in this paper, utilizing the disturbance level of AC bus voltage, has shown a notable effect in suppressing commutation failures. Table 1 illustrates the optimal startup threshold and

upper limit for various control and protection systems. It is evident that different control and protection systems significantly influence the startup threshold and upper limit values.

Table 1. Influence of control system on the optimal starting threshold and upper limit of the amplitude.

Project	CIGRE Standard Project	Linfeng HVDC Project	Fufeng HVDC Project
Optimal starting threshold	0.06	0.13	0.1
Optimal upper limit of amplitude	0.4	0.25	0.6
Effective rate	56.6%	45.0%	37.3%

Taking the CIGRE standard DC system as an example, the optimal startup thresholds and suppression effects for single-phase ground faults under different SCRs are presented in Table 2. The optimal startup thresholds vary for different AC grids, indicating that the characteristics of the AC grid in question impact the key parameters of this suppression strategy. However, overall, the variations are not substantial. Additionally, there are some efficiency differences in the effectiveness of this strategy for different AC grids under optimal configurations.

Table 2. Influence of the AC system on the optimal starting threshold.

Capacity Ratio	Optimal Starting Threshold	Original Failure Condition	New Failure Condition	Effective Rate
2.5	0.06	117	54	53.8%
5	0.06	76	33	56.6%
8	0.02	53	17	67.9%
10	0.04	43	16	62.8%

From the aforementioned research outcomes, it is apparent that the application effectiveness of this suppression strategy is constrained by the startup threshold and upper limit. These two parameters, in turn, are significantly influenced by the control and protection systems as well as the characteristics of the AC power grid.

6. Conclusions and Discussion

Based on measured transient voltage disturbance data caused by AC system faults, this paper analyzed the correlation between transient AC voltage disturbances and commutation failures in DC engineering. It was found that there exists a strong correlation between transient AC voltage disturbances caused by AC system faults and the occurrence of commutation failures in DC engineering.

Building upon this analysis, this paper proposed a real-time commutation failure suppression measure in DC transmission engineering based on transient AC bus voltage disturbances. Through fault-scanning simulations conducted on three typical control and protection systems—the CIGRE standard DC control and protection system, the XJ-SIMENS control and protection system, and the NARI-ABB control and protection system—it was observed that this measure effectively mitigated the commutation failure phenomenon induced by AC disturbances in DC systems. Notably, it showcased the best suppression effect in the Linfeng DC system.

Furthermore, the effectiveness of this suppression measure was verified through simulation using recent commutation failure fault recording data from the Linfeng and Fufeng DC transmission projects. The results demonstrated the measure's efficiency in effectively suppressing commutation failure incidents in DC projects caused by AC disturbances.

The application effectiveness of this suppression strategy is determined by startup thresholds and upper limits, parameters significantly influenced by the control and protection systems as well as the characteristics of the AC power grid. Hence, in practical applications, establishing simulation models based on different DC engineering and AC

power grid scenarios is recommended. Real-time simulations conducted under different combinations of startup thresholds and upper limits can determine the optimal parameter values for this strategy.

Author Contributions: Conceptualization, D.Z., H.H., Z.H. and L.C.; methodology, D.Z., S.H. and Y.L.; software, S.H. and Y.L.; validation, D.Z.; formal analysis, S.H. and Y.L.; investigation, D.Z., S.H. and Y.L.; resources, D.Z., H.H., Z.H. and L.C.; data curation, D.Z.; writing—original draft preparation, D.Z., S.H. and Y.L.; writing—review and editing, D.Z., S.H. and Y.L.; visualization, H.H.; supervision, Z.H.; project administration, D.Z.; funding acquisition, D.Z. All authors have read and agreed to the published version of the manuscript.

Funding: This work was supported in part by the Research Project of State Grid Shanghai Electrical Power Corporation, Research on Electromagnetic Transient Characteristics Identification and Operation-Maintenance Technology of Controlled Line-commutated Converter (CLCC) and Access System (520940230002).

Data Availability Statement: Data are contained within the article.

Conflicts of Interest: The authors declare no conflicts of interest.

References

1. Tang, Y.; Zheng, C. Review on influencing factors of commutation failure in HVDC systems. *Proc. CSEE* **2019**, *39*, 499–513.
2. Felipe, R.D.A.; Bassini, M.T.; Horita, M.A.; Jardini, J.A.; Graham, J.F.; Liu, G. HVDC multi-infeed analysis of the Brazilian transmission system and possible mitigation methods. *CSEE J. Power Energy Syst.* **2018**, *4*, 487–494.
3. Mirsaeidi, S.; Tzelepis, D.; He, J.; Dong, X.; Said, D.M.; Booth, C. A Controllable Thyristor-Based Commutation Failure Inhibitor for LCC-HVDC Transmission Systems. *IEEE Trans. Power Electron.* **2020**, *36*, 3781–3792. [CrossRef]
4. Ouyang, J.; Zhang, Z.; Li, M.; Pang, M.; Xiong, X.; Diao, Y. A Predictive Method of LCC-HVDC Continuous Commutation Failure Based on Threshold Commutation Voltage Under Grid Fault. *IEEE Trans. Power Syst.* **2020**, *36*, 118–126. [CrossRef]
5. Nazir, M.; Enslin, J.H. Hybrid Smart Converter Transformer for Enhanced HVDC Reliability and Reduced Complexity. In Proceedings of the 2020 4th International Conference on HVDC (HVDC), Xi'an, China, 6–9 November 2020; pp. 742–748.
6. Guo, C.; Zhao, J.; Liu, W.; Yang, Z.; Zhao, C. A review of methods to mitigate the commutation failure for LCC-HVDC. *Proc. CSEE* **2018**, *38* (Suppl. 1), 1–10.
7. Majid, Z.S.; Arief, A.; Akil, Y.S. Minimization of Transmission Loss in Application of HVDC Networks under Load Increase Scenario. *Int. J. Electr. Electron. Eng. Telecommun.* **2021**, *10*, 333–340. [CrossRef]
8. Ohuchi, K.; Masod, A.F.B.; Kato, S.; Hirase, Y. Stability Assessment of a High-Voltage DC Transmission System Using MIMO- and SISO-Based Impedances. *Int. J. Electr. Electron. Eng. Telecommun.* **2023**, *12*, 71–80. [CrossRef]
9. Gnudi, R.; Giannuzzi, G.; Pisani, C.; Noce, M.; Porcu, A.; Coletta, G. Commutation Failure Immunity Monitoring: The Italian Operation Experience. In Proceedings of the 2023 AEIT HVDC International Conference (AEIT HVDC), Rome, Italy, 25–26 May 2023; pp. 1–6.
10. Mirsaeidi, S.; Liu, H.; He, J.; Tzelepis, D.; Said, D.M. Reduction of commutation failure frequency in HVDC transmission systems by means of an improved solid-state fault current limiter. In Proceedings of the 2020 IEEE Sustainable Power and Energy Conference (iSPEC), Chengdu, China, 23–25 November 2020; pp. 2493–2499.
11. Liu, L.; Lin, S.; Sun, P.; Liao, K.; Li, X.; Deng, Y.; He, Z. A Calculation Method of Pseudo Extinction Angle for Commutation Failure Mitigation in HVDC. *IEEE Trans. Power Deliv.* **2019**, *34*, 777–779. [CrossRef]
12. Rehman, B.; Liu, C.; Li, H.; Fu, C.; Wei, W. Analysis on local and concurrent commutation failure of multi-infeed HVDC considering inter-converter interaction. *J. Mod. Power Syst. Clean Energy* **2021**, *10*, 1050–1059. [CrossRef]
13. Xue, Y.; Zhang, X.P.; Yang, C. Commutation failure elimination of LCC HVDC systems using thyristor-based controllable capacitors. *IEEE Trans. Power Deliv.* **2017**, *33*, 1448–1458. [CrossRef]
14. De Toledo Silva, F.A.; Komatsu, W.; Pedroso, F.V.; Jardini, J.A.; Bélanger, J. Faster-than-Real-Time Simulation of a Large Brazilian AC/DC Grid to Analyze Electromagnetic & Electromechanical Transients as Well as Commutation Failures. In Proceedings of the 2020 IEEE PES Transmission & Distribution Conference and Exhibition-Latin America (T&D LA), Montevideo, Uruguay, 29 September–1 October 2020; pp. 1–6.
15. Zhu, R.; Zhou, X.; Xia, H.; Hong, L.; Yin, H.; Deng, L.; Liu, Y. Commutation Failure Mitigation Method Based on Imaginary Commutation Process. *J. Mod. Power Syst. Clean Energy* **2022**, *10*, 1413–1422. [CrossRef]
16. Chen, S.; Li, X.; Yu, J.; Li, T.; Lu, P.; Yin, Y. A method based on the sin-cos components detection mitigates commutation failure in HVDC. *Proc. Chin. Soc. Electr. Eng.* **2005**, *25*, 1.
17. Wei, Z.; Fang, W.; Liu, J. Variable Extinction Angle Control Strategy Based on Virtual Resistance to Mitigate Commutation Failures in HVDC System. *IEEE Access* **2020**, *8*, 93692–93704. [CrossRef]
18. Lee, C.; Shim, J.W.; Kim, H.; Hur, K. DC Power Control Strategy of MMC for Commutation Failure Prevention in Hybrid Multi-Terminal HVDC System. *IEEE Access* **2020**, *8*, 180576–180586. [CrossRef]

19. Zhou, B.; Li, F.; Song, X.; Yin, C. Commutation failure prediction and control system optimization based on DC current variation. *Power Syst. Technol.* **2019**, *43*, 1–8.
20. Cunha, A.C.; Leal, G.; Aredes, M.; Alves, F.; Souza, M.J. Static-Based Analytical Approach to Quantify the Power Dispatch Influence on LCC-HVDCs Resilience to Commutation Failure. In Proceedings of the 2023 IEEE 8th Southern Power Electronics Conference (SPEC), Florianopolis, Brazil, 26–29 November 2023; pp. 1–8.
21. Mirsaeidi, S.; Giramata, A.; Tzelepis, D.; He, J.; Said, D.M.; Muttaqi, K.M. An Introspective Review on Commutation Failure Inhibition Strategies in LCC-HVDC Transmission Networks. In Proceedings of the 2022 IEEE Industry Applications Society Annual Meeting (IAS), Detroit, MI, USA, 9–14 October 2022; pp. 1–7.
22. Wang, F.; Liu, T.; Zhou, S.; Li, X.; Qiao, G. Mechanism and quantitative analysis method for HVDC commutation failure resulting from harmonics. *Proc. CSEE* **2015**, *35*, 4888–4894.
23. Awan, F.G.; Anwarr, B.; Omer, M.; Zubair, M.; Altaf, M.W.; Ahmad, W.; Kiran, A. Parametric Modeling of Resistive type Super-conducting FCL for Commutation Failure Improvement in HVDC System. In Proceedings of the 2022 International Conference on Electrical Engineering and Sustainable Technologies (ICEEST), Lahore, Pakistan, 14–15 December 2022; pp. 1–5.